

# We are IntechOpen, the world's leading publisher of Open Access books Built by scientists, for scientists

6,900

Open access books available

186,000

International authors and editors

200M

Downloads

Our authors are among the

154

Countries delivered to

TOP 1%

most cited scientists

12.2%

Contributors from top 500 universities



WEB OF SCIENCE™

Selection of our books indexed in the Book Citation Index  
in Web of Science™ Core Collection (BKCI)

Interested in publishing with us?  
Contact [book.department@intechopen.com](mailto:book.department@intechopen.com)

Numbers displayed above are based on latest data collected.  
For more information visit [www.intechopen.com](http://www.intechopen.com)



# Ab Initio Hamiltonian Approach to Light-Front Quantum Field Theory

James P. Vary  
*Department of Physics and Astronomy, Iowa State University, Ames, Iowa*  
 USA

## 1. Introduction

Non-perturbative solutions of quantum field theory represent opportunities and challenges that span particle physics and nuclear physics. Increasingly, it is also gaining attention in condensed matter physics. Fundamental understanding of, among others, the phase structure of strongly interacting systems, the spin structure of the proton, the neutron electromagnetic form factor, and the generalized parton distributions of the baryons should emerge from results derived from a non-perturbative light-front Hamiltonian approach. The light-front Hamiltonian quantized within a basis function approach as described here offers a promising avenue that capitalizes on theoretical and computational achievements in quantum many-body theory over the past decade.

By way of background, one notes that Hamiltonian light-front field theory in a discretized momentum basis (1) and in transverse lattice approaches (2; 3) have shown significant promise. I outline here a Hamiltonian basis function approach following Refs. (4–10) that exploits recent advances in solving the non-relativistic strongly interacting nuclear many-body problem (11; 12). There are many issues faced in common - i.e. how to (1) define the Hamiltonian; (2) renormalize for the available finite spaces while preserving all symmetries; (3) solve for eigenvalues and eigenvectors; (4) evaluate experimental observables; and, (5) take the continuum limit.

I begin with a brief overview of recent advances in solving light nuclei with realistic nucleon-nucleon (NN) and three-nucleon (NNN) interactions using *ab initio* no-core methods. After reviewing some advances with two-dimensional theories, I outline a basis function approach suitable for light front gauge theories including the issues of renormalization/regularization. I present an introduction to the approach for cavity-mode QED, to systems in the absence of an external cavity and I discuss its extension to QCD.

## 2. No Core Shell Model (NCSM) and No Core Full Configuration (NCFC) methods

To solve for the properties of self-bound strongly interacting systems, such as nuclei, with realistic Hamiltonians, one faces immense theoretical and computational challenges. Recently, *ab initio* approaches have been developed that treat all the nucleons on an equal footing, preserve all the underlying symmetries and converge to the exact result given sufficient computational effort. The basis function approach (11; 12) is one of several methods shown to be successful. The primary advantages are its flexibility for choosing the Hamiltonian, the

method of renormalization/regularization and the basis space. These advantages support the adoption of the basis function approach in light-front quantum field theory.

Refs. (11; 13–18) and (12; 19; 20) provide examples of the recent advances in the *ab initio* NCSM and NCFC, respectively. The NCSM adopts a renormalization method that provides an effective interaction dependent on the chosen many-body basis space (e.g. on the harmonic oscillator length scale) and on its cutoff ( $N_{max}$  below). The NCFC either retains the un-renormalized interaction or adopts a basis-space independent renormalization so that the exact results are obtained either by using a sufficiently large basis space or by extrapolation to the infinite matrix limit. Recent results for the NCSM employ realistic nucleon-nucleon (NN) and three-nucleon (NNN) interactions derived from chiral effective field theory to solve nuclei with Atomic Numbers 10-13 (15) and Atomic Number 14 (17). For an overview of the NCSM including applications to reactions and to effective interactions with a core, see Ref. (18). Recent results for the NCFC feature a realistic NN interaction that is sufficiently soft that binding energies and spectra from a sequence of finite matrix solutions may be extrapolated to the infinite matrix limit (20). Experimental binding energies, spectra, magnetic moments and Gamow-Teller transition rates are well-reproduced in both the NCSM and NCFC approaches. Convergence of long range observables such as the RMS radius and the electric quadrupole are more challenging since they are sensitive to the exponential tails of the nuclear wavefunctions.

It is important to note two recent analytical and technical advances. First, non-perturbative renormalization has been developed to accompany these basis-space methods and their success is impressive. Several schemes have emerged and current research focuses on understanding of the scheme-dependence of convergence rates. Among the many issues to consider, I note that different observables converge at different rates (19) even within a fixed scheme. Second, large scale calculations are performed on leadership-class parallel computers to solve for the low-lying eigenstates and eigenvectors and to evaluate a suite of experimental observables. Low-lying solutions for matrices of basis-space dimension 10-billion on 215,000 cores with a 5-hour run is the current record. However, one expects these limits to continue growing as the techniques are evolving rapidly (16) and the computers are also growing dramatically. Matrices with dimensions in the several tens of billions will soon be solvable with strong interaction Hamiltonians. Note, however, that it is not simply the matrix dimension that controls the level of the computational challenge but a set of issues that includes the sparsity of the Hamiltonian matrix (which depends dramatically on whether NNN interactions are employed), the density of the eigenvalue spectrum, the range of excitation energies desired, etc.

In a NCSM or NCFC application, one adopts a 3D harmonic oscillator (HO) with HO energy  $\omega$  (using  $\hbar = 1$  units) for all the particles in the nucleus, treats the neutrons and protons independently, and generates a many-fermion basis space that includes the lowest oscillator configurations as well as all those generated by allowing up to  $N_{max}$  oscillator quanta of excitations. The single-particle states specify the orbital angular momentum projection and the basis is referred to as the  $m$ -scheme basis. For the NCSM one also selects a renormalization scheme linked to the basis truncation while in the NCFC the renormalization is either absent or of a type that retains the infinite matrix problem. In the NCFC case (12), one either proceeds to a sufficiently large basis that converged results are obtained (if that is computationally feasible) or extrapolates to the continuum limit as I now illustrate.

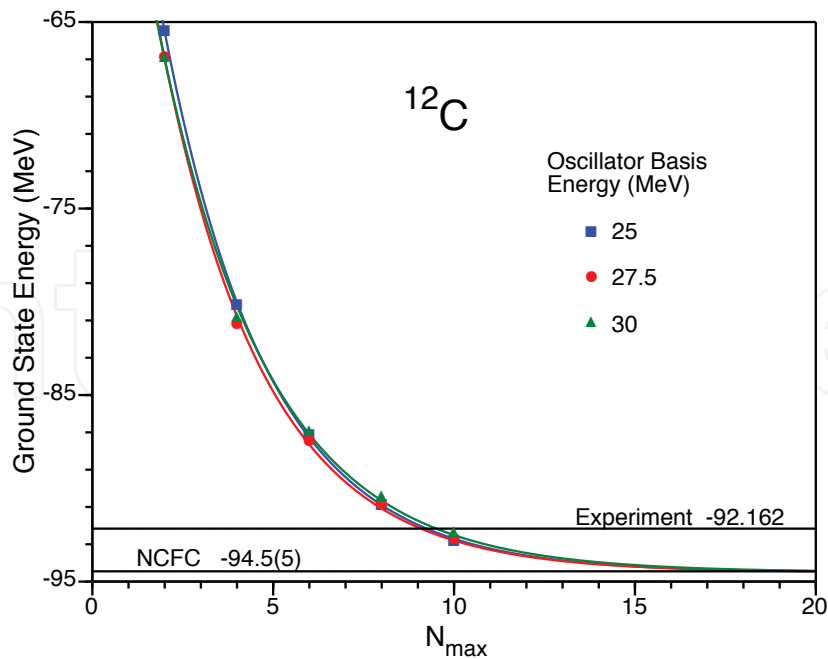


Fig. 1. (Color online) Calculated ground state (gs) energy of  $^{12}\text{C}$  for  $N_{max} = 2-10$  (symbols) at selected values of  $\omega$  indicated in the legend. For each  $\omega$ , the results are fit to an exponential plus a constant, the asymptote, constrained to be the same for all  $\omega$ (12). Horizontal lines indicate the experimental gs and the NCFC result (uncertainty = 0.5 MeV).

I show in Fig. 1 results for the ground state (gs) of  $^{12}\text{C}$  as a function of  $N_{max}$  obtained with a realistic NN interaction, JISP16 (14). The smooth curves portray fits that achieve asymptotic independence of  $N_{max}$  and  $\omega$ . The NCFC gs energy (the common asymptote) of  $-94.5$  MeV indicates  $\sim 3\%$  overbinding. The assessed uncertainty in the NCFC result is 0.5 MeV indicated in parenthesis in the figure. The largest  $^{12}\text{C}$  calculations correspond to  $N_{max} = 10$ , with a matrix dimension near 8 billion.  $N_{max} = 12$  produces a matrix dimension near 81 billion which we hope to solve in the future.

In order to further illustrate the successes of the *ab initio* NCSM, I display in Fig. 2 the natural-parity excitation spectra of four nuclei in the middle of the  $0p$ -shell with both the NN and the NN+NNN effective interactions from  $\chi\text{EFT}$  (15). Overall, the NNN interaction contributes significantly to improve theory in comparison with experiment. This is especially well-demonstrated in the odd mass nuclei for the lowest, few excited states. The case of the g.s. spin of  $^{10}\text{B}$  and its sensitivity to the presence of the NNN interaction is clearly evident. The results of numerous *ab initio* NCSM applications not only show good convergence with regard to increasing size of the basis space but also have reproduced known properties of  $0p$ -shell nuclei (nuclei up to  $^{16}\text{O}$ ) as well as explained existing puzzles and made predictions of, as yet, unexplained nuclear phenomena. I cite another prominent example to illustrate this point.

We recently evaluated the Gamow-Teller (GT) matrix element for the beta decay of  $^{14}\text{C}$ , including the effect of chiral NNN forces (17). These investigations showed that the very long lifetime for  $^{14}\text{C}$  arises from a cancellation between  $0p$ -shell NN-and NNN-interaction contributions to the GT matrix element, as shown in Figure 3. The net result is a GT matrix

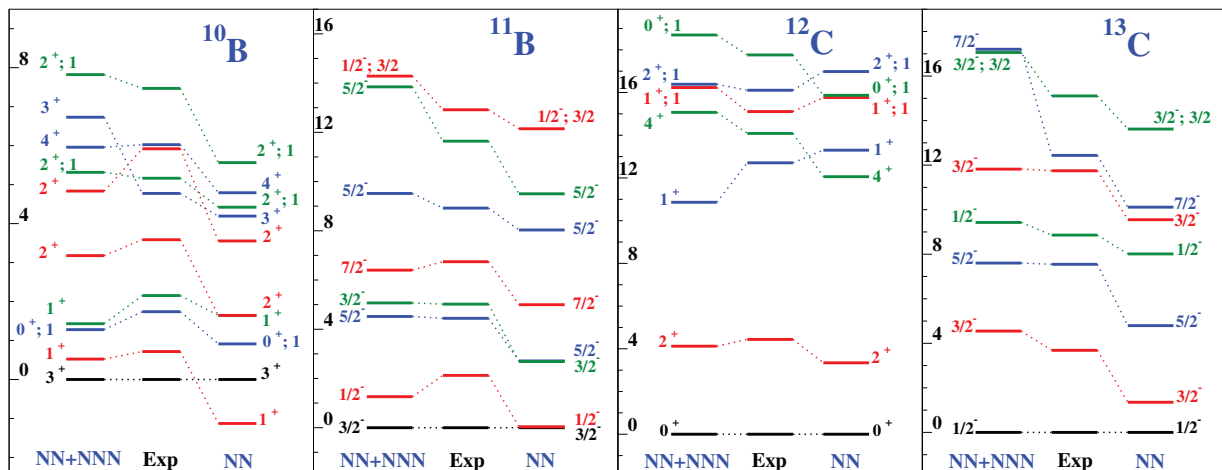


Fig. 2. States dominated by  $0p$ -shell configurations for  $^{10}\text{B}$ ,  $^{11}\text{B}$ ,  $^{12}\text{C}$ , and  $^{13}\text{C}$  calculated at  $N_{\text{max}} = 6$  using  $\hbar\Omega = 15$  MeV (14 MeV for  $^{10}\text{B}$ ). Most of the eigenstates are isospin  $T=0$  or  $1/2$ , the isospin label is explicitly shown only for states with  $T=1$  or  $3/2$ . The excitation energy scales are in MeV (adopted from Ref (15)).

element close to zero (final point of the green curve in the lower half of Fig. 3) which is far more consistent with the 5730 year half-life of  $^{14}\text{C}$ . The same calculations show that including the NNN-interactions also bring the binding energies of  $^{14}\text{C}$  and  $^{14}\text{N}$  into closer agreement with experiment. These  $A=14$  beta decay results were obtained in the largest basis space achieved to date with NNN interactions,  $N_{\text{max}} = 8$ , or approximately one billion m-scheme configurations.

Other noteworthy results include calculations for  $^{12}\text{C}$  explaining the measured  $^{12}\text{C}$  B(M1) transition from the g.s. to the  $(1^+, 1)$  state at 15.11 MeV and showing more than a factor of 2 enhancement arising from the NNN interaction (13). Neutrino elastic and inelastic cross sections on  $^{12}\text{C}$  were shown to be similarly sensitive to the NNN interaction and their contributions significantly improve agreement with experiment (13). Working in collaboration with experimentalists, we uncovered a puzzle in the GT-excited state strengths in  $A=14$  nuclei (21). Its resolution may lie in the role of intruder-state admixtures, but this will require further work.

In addition to numerous successful applications to spectra and electroweak transitions in light nuclei, major efforts are underway to develop extensions to *ab initio* nuclear reactions(18). Key motivations include the goal to further refine our understanding of the fundamental strong interactions among the constituent nucleons and to provide, at the same time, accurate predictions of crucial reaction rates for nuclear astrophysics.

An *ab initio* approach to nuclear reactions based on the NCSM requires a precise treatment of the wave-function asymptotics and the coupling to the continuum. These requirements have led to a new approach, the *ab initio* NCSM/RGM (22; 23), capable of simultaneously describing both bound and scattering states in light nuclei, by combining the resonating-group method (RGM) (24) with the *ab initio* NCSM. The RGM is a microscopic cluster technique based on the use of  $A$ -nucleon Hamiltonians, with fully anti-symmetric many-body wave functions built assuming that the nucleons are grouped into clusters. By combining the NCSM with the RGM, one complements the ability of the RGM to deal with scattering and reactions with the utilization of realistic interactions and a consistent *ab initio* microscopic description of

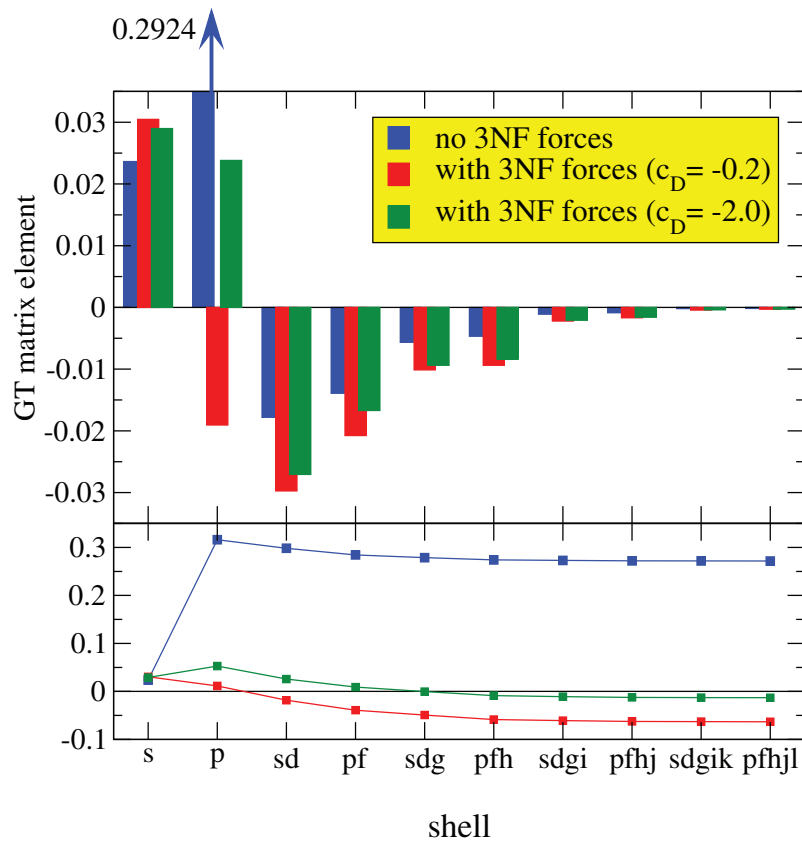


Fig. 3. (Color online) Contributions to the  $^{14}\text{C}$  beta decay matrix element as a function of the 3D harmonic oscillator shell in the basis space when the nuclear structure is described by the  $\chi\text{EFT}$  interaction (adopted from Ref. (17)). Top panel displays the contributions with (two right bars, the red and green, of each triplet) and without (leftmost bar, the blue bar, of each triplet) the NNN force at  $N_{\text{max}} = 8$ . Contributions are summed within each shell to yield a total for that shell. The bottom panel displays the running sum of the GT contributions over the shells with the same color coding scheme. Two reasonable choices for coupling constants (red and green components of the histogram and lines) in the NNN-interaction lead to similar strong suppression of the GT matrix element. Note, in particular, the order-of-magnitude suppression of the  $0p$ -shell contributions arising from the NNN force.

the nucleonic clusters, while preserving important symmetries, including the Pauli exclusion principle and translational invariance.

### 3. Light-front Hamiltonian field theory

It has long been known that light-front Hamiltonian quantum field theory has similarities with non-relativistic quantum many-body theory and this has prompted applications with established non-relativistic many-body methods (see Ref. (1) for a review). These applications include theories in 1+1, 2+1 and 3+1 dimensions. Several of my efforts in 1+1 dimensions, in collaboration with others, have focused on developing an understanding of how one detects and characterizes phase transition phenomena in the Hamiltonian approach. To this end, I list the following developments:

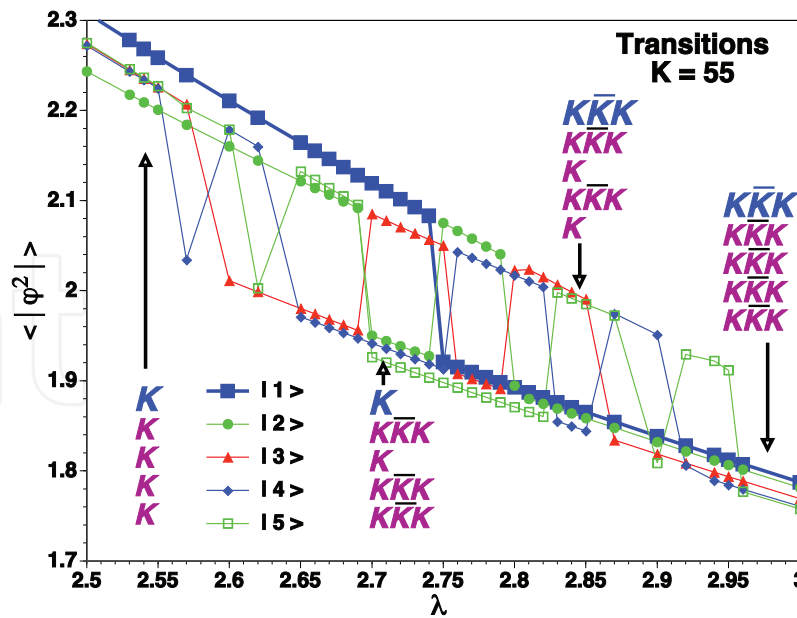


Fig. 4. Expectation value of the square of the scalar field as a function of the coupling constant  $\lambda$  at light-front harmonic resolution  $K=55$  for the lowest five excitations of two dimensional  $\phi^4$  in the broken phase (27). The pattern of transitions correspond to 5 states falling with increasing  $\lambda$  and crossing the 5 lowest states, thus replacing them and becoming the new 5 lowest states. At selected values of  $\lambda$ , the character of the lowest states is indicated on the figure with the top level of each column signifying the nature of the lowest state. Successive excited states are signified by the labels proceeding down the column. The letter “K” represents “kink” while “ $K\bar{K}$ ” represents “kink-antikink-kink”.

1. identification and characterization of the quantum kink solutions in the broken symmetry phase of two dimensional  $\phi^4$  including the extraction of the vacuum energy and kink mass that compare well with classical and semi - classical results (25);
2. detailed investigation of the strong coupling region of the topological sector of the two-dimensional  $\phi^4$  theory demonstrating that low-lying states with periodic boundary conditions above the transition coupling are dominantly kink-antikink coherent states (26);
3. switching to anti-periodic boundary conditions in the strong coupling region of the topological sector of the two-dimensional  $\phi^4$  theory and demonstrating that low-lying states above the critical coupling are dominantly kink-antikink-kink states as well as presenting evidence for the onset of kink condensation(27). Fig. 4 presents the detailed transition of the lowest 5 mass eigenstates in the broken phase from kink to kink-antikink-kink structure over a narrow range in the coupling. Increasing the resolution  $K$  shrinks the range in coupling over which the transitions occur.

More recently, full-fledged applications to gauge theories in 3+1 dimensions have appeared along with roadmaps for addressing QCD. A brief summary of some of the major developments in 3+1 dimensional Hamiltonian light front field theory includes the solutions of:

1. light-front QED wave equations for the electron plus electron-photon system (28–30)
2. simplified gauge theories with a transverse lattice (2; 3; 31)

3. Hamiltonian QED for the electron plus electron-photon system in a trap with a basis function approach (4; 7; 8) that I discuss in the next section.
4. Hamiltonian QED for the electron plus electron-photon system without an external trap that I also discuss in the next section(9; 10)

These successes open pathways for ambitious research programs to evaluate non-perturbative amplitudes and to address the multitude of experimental phenomena that are conveniently evaluated in a light-front quantized approach. As one important example, consider the deeply virtual Compton scattering (DVCS) process which provides the opportunity to study the 3-dimensional coordinate space structure of the hadrons. Recent efforts with model 3+1 dimensional light-front amplitudes (32) have shown that the Fourier spectra of DVCS should reveal telltale diffractive patterns indicating detailed properties of the coordinate space structure.

Additional applications include the non-perturbative regime of QED that future experiments with ultra-strong pulsed lasers will explore, for example, looking for non-perturbative lepton pair production (33–35). Yet another application resides with the strong time-dependent QED fields generated in relativistic heavy-ion collisions where puzzling excesses of electron-positron pairs have been observed (36; 37).

#### 4. Basis light-front quantization applied to QED

We define our light-front coordinates as  $x^\pm = x^0 \pm x^3$ ,  $x^\perp = (x^1, x^2)$ , where the variable  $x^+$  is light-front time and  $x^-$  is the longitudinal coordinate. We adopt  $x^+ = 0$ , the “null plane”, for our quantization surface. Here we adopt basis states for each constituent that consist of transverse 2D harmonic oscillator (HO) states combined with discretized longitudinal modes, plane waves, satisfying selected boundary conditions. This basis function approach follows Refs. (4–6). Note that the choice of basis functions is arbitrary except for the standard conditions of orthonormality and completeness. Adoption of this particular basis is consistent with recent developments in AdS/QCD correspondence with QCD (38; 39).

The HO states are characterized by a principal quantum number  $n$ , orbital quantum number  $m$ , and HO energy. Here we adopt the convention that  $\Omega$  represents both the energy of the transverse HO trap and the basis representation when the trap is present (i.e we match the basis to the trap potential). To signal that the trap is absent we use  $\omega$  to represent the frequency choice for the basis.

Working in momentum space, it is convenient to write the 2D oscillator as a function of the dimensionless variable  $\rho = |p^\perp| / \sqrt{M_0 \Omega}$ , and  $M_0$  has units of mass. The orthonormalized HO wave functions in polar coordinates  $(\rho, \varphi)$  are then given in terms of the generalized Laguerre polynomials,  $L_n^{|m|}(\rho^2)$ , by

$$\begin{aligned} \Phi_{nm}(\rho, \varphi) &= \langle \rho \varphi | nm \rangle \\ &= \sqrt{\frac{2\pi}{M_0 \Omega}} \sqrt{\frac{2n!}{(|m| + n)!}} e^{im\varphi} \rho^{|m|} e^{-\rho^2/2} L_n^{|m|}(\rho^2), \end{aligned} \quad (1)$$

with HO eigenvalues  $E_{n,m} = (2n + |m| + 1)\Omega$ . The HO wavefunctions have the same analytic structure in both coordinate and momentum space, a feature reminiscent of a plane-wave basis.

The longitudinal modes,  $\psi_k$ , in our basis are defined for  $-L \leq x^- \leq L$  with periodic boundary conditions for the photon and antiperiodic boundary conditions for the electron:

$$\psi_k(x^-) = \frac{1}{\sqrt{2L}} e^{i \frac{\pi}{L} k x^-}, \quad (2)$$

where  $k = 1, 2, 3, \dots$  for periodic boundary conditions (we neglect the zero mode) and  $k = \frac{1}{2}, \frac{3}{2}, \frac{5}{2}, \dots$  for antiperiodic boundary conditions. The full 3D single-particle basis state is defined by the product form

$$\Psi_{k,n,m}(x^-, \rho, \varphi) = \psi_k(x^-) \Phi_{n,m}(\rho, \varphi). \quad (3)$$

For illustrative purposes, we select a transverse mode with  $n = 1, m = 0$  joined together with the  $k = \frac{1}{2}$  longitudinal antiperiodic boundary condition mode of Eq. 2 and display slices of the real part of this 3-D basis function at selected longitudinal coordinates,  $x^-$  in Fig. 5. For comparison, we present a second example with box boundary conditions for the longitudinal mode in Fig. 6. Our purpose in presenting both Figs. 5 and 6 is to suggest the richness, flexibility and economy of texture available for solutions in a basis function approach.

Next, we introduce the total invariant mass-squared  $M^2$  for the low-lying physical states in terms of a Hamiltonian  $H$  times a dimensionless integer for the total light-front momentum  $K$

$$M^2 + P_\perp P_\perp \rightarrow M^2 + const = P^+ P^- = KH \quad (4)$$

where we absorb the constant into  $M^2$ . For simplicity, the transverse functions for both the electron and the photon were taken as eigenmodes of the external trap in our initial application (7) which we discuss here (below, we present results with the external trap removed). The noninteracting Hamiltonian  $H_0 = 2M_0 P_c^-$  for this system with a trap is then defined by the sum of the occupied modes  $i$  in each many-parton state:

$$H_0 = \frac{2M_0 \Omega}{K} \sum_i \frac{2n_i + |m_i| + 1 + \bar{m}_i^2 / (2M_0 \Omega)}{x_i}, \quad (5)$$

where  $\bar{m}_i$  is the mass of the parton  $i$ . The photon mass is set to zero throughout this work and the electron mass  $\bar{m}_e$  is set at the physical mass 0.511 MeV in our nonrenormalized calculations. We also set  $M_0 = \bar{m}_e$ .

The light-front QED Hamiltonian interaction terms we need are the electron to electron-photon vertex, given as

$$V_{e \rightarrow e\gamma} = g \int dx_+ d^2 x_\perp \bar{\Psi}(x) \gamma^\mu \Psi(x) A_\mu(x) \Big|_{x^+=0}, \quad (6)$$

and the instantaneous electron-photon interaction,

$$V_{e\gamma \rightarrow e\gamma} = \frac{g^2}{2} \int dx_+ d^2 x_\perp \bar{\Psi} \gamma^\mu A_\mu \frac{\gamma^+}{i\partial^+} (\gamma^\nu A_\nu \Psi) \Big|_{x^+=0}, \quad (7)$$

where the coupling constant  $g^2 = 4\pi\alpha$ , and  $\alpha$  is the fine structure constant. The nonspinflip vertex terms of Eq.(6) are  $\propto M_0 \Omega$ , whereas spinflip terms are  $\propto \sqrt{M_0 \Omega} m_e$ . Selecting the initial state electron helicity in the single electron sector always as "up" the process  $e \rightarrow e\gamma$  is nonzero

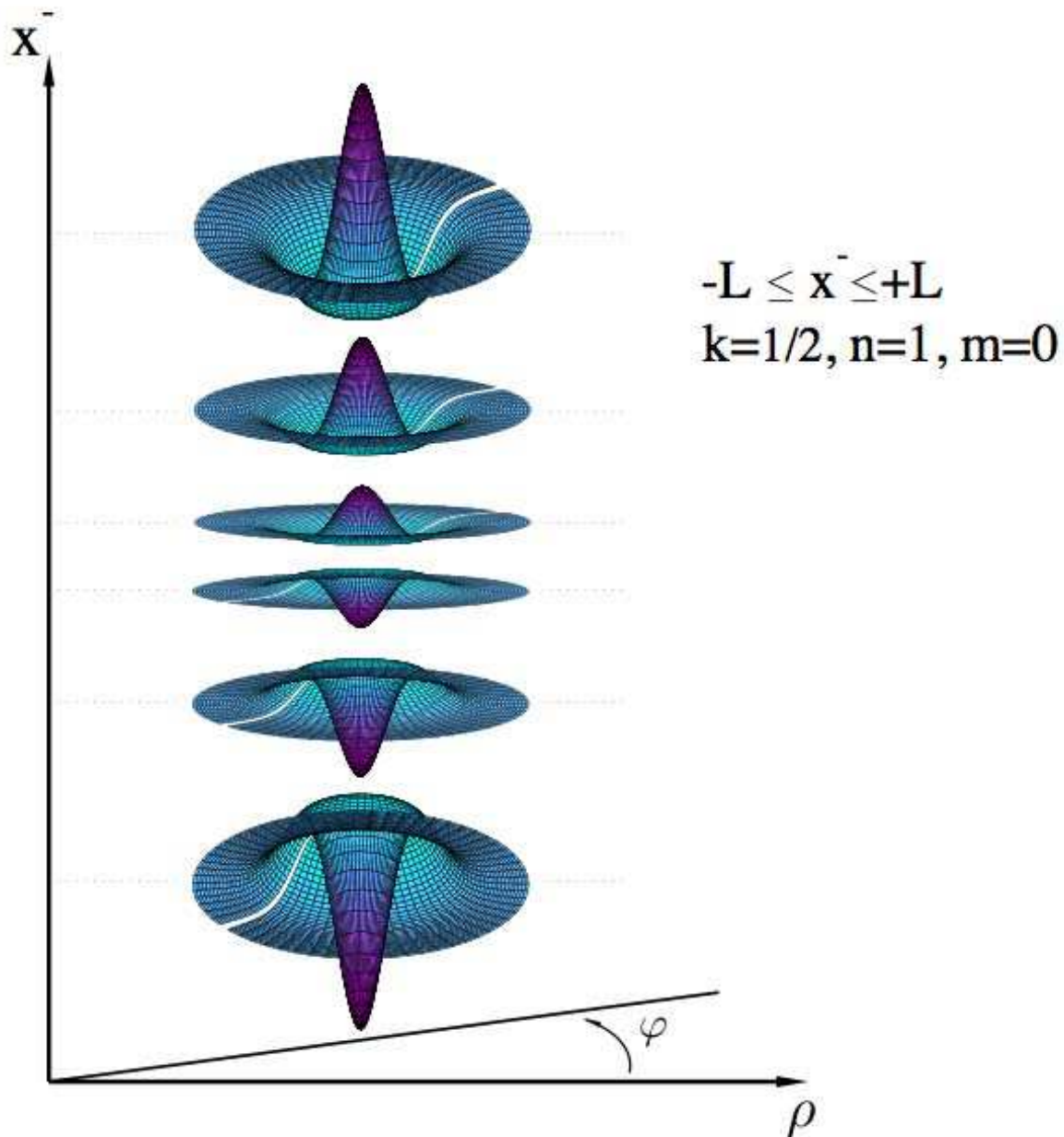


Fig. 5. (color online) Transverse sections of the real part of a 3-D basis function involving a 2-D harmonic oscillator and a longitudinal mode of Eq. 2 with antiperiodic boundary conditions. The quantum numbers for this basis function are given in the legend. The basis function is shown for the full range  $-L \leq x^- \leq L$  (adapted from Ref. (4)).

for three out of eight helicity combinations, and the process  $e\gamma \rightarrow e\gamma$  is nonzero only with all four spin projections aligned (two out of 16 combinations), resulting in a sparse matrix.

We implement a symmetry constraint for the basis by fixing the total angular momentum projection  $J_z = M + S = \frac{1}{2}$ , where  $M = \sum_i m_i$  is the total azimuthal quantum number, and  $S = \sum_i s_i$  the total spin projection along the  $x^-$  direction. For cutoffs, we select the total light-front momentum,  $K$ , and the maximum total quanta allowed in the transverse mode of

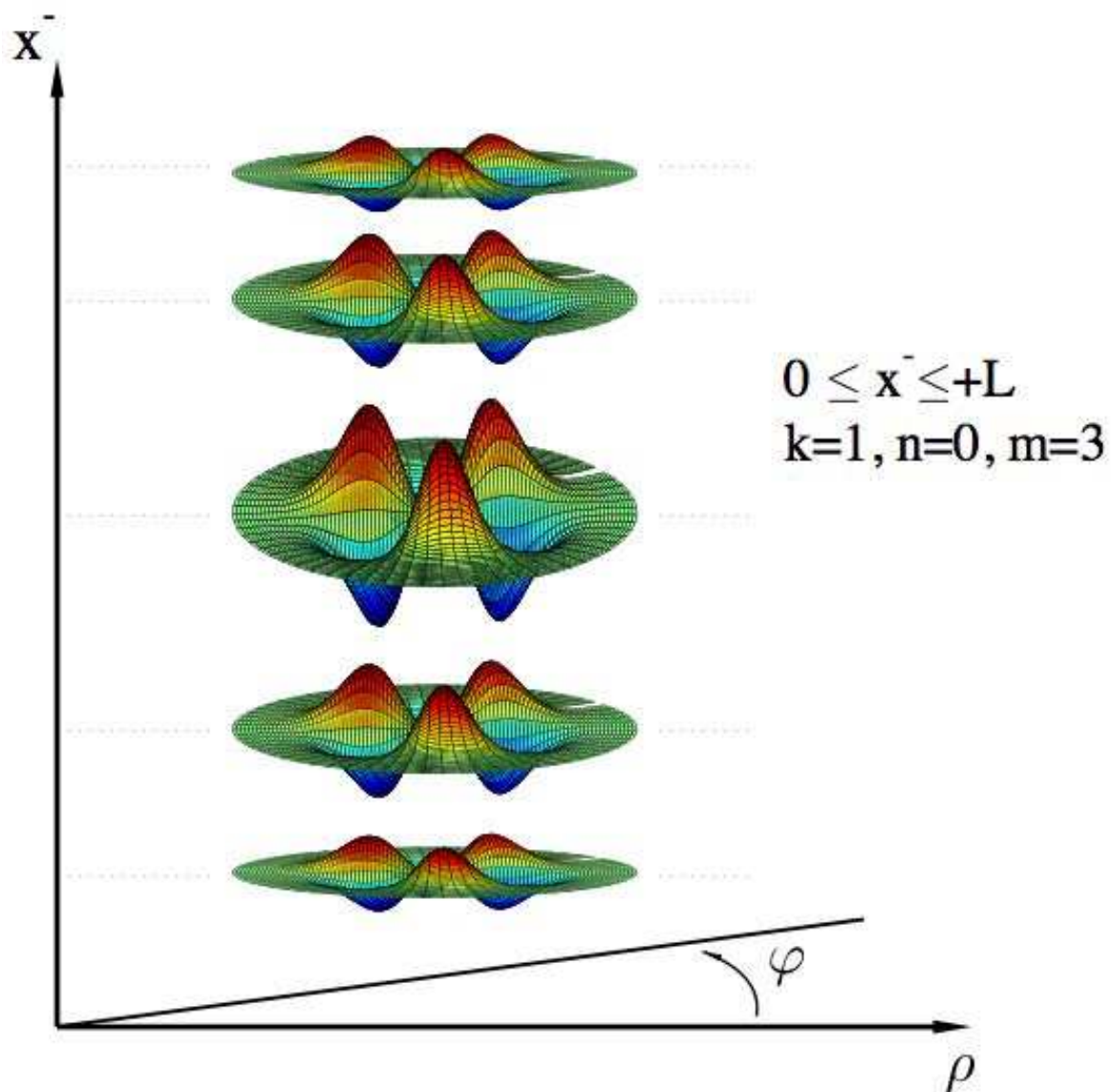


Fig. 6. (color online) Transverse sections of a 3-D basis function involving a 2-D harmonic oscillator and a longitudinal mode with box boundary conditions (wavefunction vanishes at  $\pm L$ ). The quantum numbers for this basis function are given in the legend. The basis function is shown for positive values of  $x^-$  and is antisymmetric with respect to  $x^- = 0$  (adapted from Ref. (4)).

each one or two-parton state,  $N_{max}$ , such that

$$\sum_i x_i = 1 = \frac{1}{K} \sum_i k_i, \quad (8)$$

$$\sum_i 2n_i + |m_i| + 1 \leq N_{max}, \quad (9)$$

where, for example,  $k_i$  defines the longitudinal modes of Eq.(2) for the  $i^{th}$  parton. Equation (8) signifies total light-front momentum conservation written in terms of boost-invariant momentum fractions,  $x_i$ . Since we employ a mix of boundary conditions and all states have

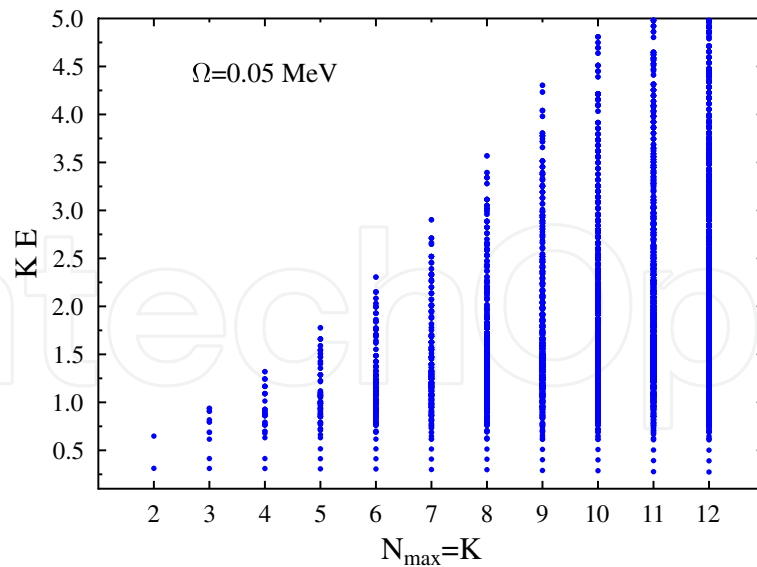


Fig. 7. (color online). Eigenvalues (multiplied by  $K$ ) for a nonrenormalized light-front QED Hamiltonian for an electron in an external trap with  $\Omega = 0.05$  MeV which includes the electron-photon vertex and the instantaneous electron-photon interaction. The cutoffs for the basis space dimensions are selected such that  $K$  increases simultaneously with the  $N_{max}$ .

half-integer total  $K$ , we will quote  $K$  values rounded downwards for convenience, except when the precise value is required.

In our approach, the HO parameters  $\Omega$ ,  $M_0$ , the electron mass  $m_e$ , and the total longitudinal momentum  $K$  appear as prefactors for the matrix elements in the Hamiltonian. Therefore, we can rather straightforwardly vary the size of the Hamiltonian matrix by keeping  $N_{max}$  fixed, and changing  $K$  alone. This facilitates examination of the convergence rates at each value of  $N_{max}$ .

In our initial applications, we focus on QED and consider a system including only  $|e\rangle$  and  $|e\gamma\rangle$  sectors in a transverse scalar harmonic trap (7) and, more recently, in the absence of the external trap (10; 40). Both of these setups, once the Fock space is extended, will be useful for addressing a range of strong field QED problems such as electron-positron pair production in relativistic heavy-ion collisions and with ultra-strong pulsed lasers planned for the future. We adopt the sector dependent non-perturbative renormalization scheme (41).

In Fig. 7 we show the eigenvalues (multiplied by  $K$ ) for a nonrenormalized light-front QED Hamiltonian given in Eqs.(5,6,7), with fixed  $\Omega = 0.05$  MeV and simultaneously increasing  $K$  and  $N_{max}$ . The resulting dimension of the Hamiltonian matrix increases rapidly. For  $N_{max} = K = 2, 10$ , and  $20$ , the dimensions of the corresponding symmetric  $d \times d$  matrices are  $d = 2, 1670$ , and  $26\ 990$ , respectively.

The number of the single electron basis states, considering all the symmetries, increases slowly with increasing  $N_{max} = K$  cutoff. For  $N_{max} = K = 2, 10$ , and  $20$  the number of single electron basis states is  $1, 5$ , and  $10$ , respectively. Our lowest-lying eigenvalue corresponds to a solution dominated by the electron with  $n = m = 0$ . The ordering of excited states, due to significant interaction mixing, does not always follow the highly degenerate unperturbed spectrum of Eq.(5). States dominated by spin-flipped electron-photon components are evident

in the solutions. Nevertheless, the lowest-lying eigenvalues appear with nearly harmonic separations in Fig. 7 as would be expected at the coupling of QED. The multiplicity of the higher eigenstates increases rapidly with increasing  $N_{max} = K$  and the states exhibit stronger mixing with other states than the lowest-lying states. In principle, the electron-photon basis states interact directly with each other in leading order through the instantaneous electron-photon interaction, but numerically the effect of this interaction is very weak, and thus does not contribute significantly to the mixing. Even though we work within a Fock-space approach, our numerical results should approximate the lowest order perturbative QED results for sufficiently weak external field.

In the most recent application to QED, we still retain the truncated basis including only  $|e\rangle$  and  $|e\gamma\rangle$  sectors as in Ref. (7). However, we introduce major extensions and improvements. For a more complete description, I refer to the paper by Zhao, et al. (10) and to a separate paper (40). Here, I simply list a few of the key extensions and improvements.

1. In order to expand the range of applications, we extend the application of BLFQ to a free space system by omitting the external transverse trap.
2. In order to improve computational efficiency and numerical precision, we replace numerical integrations previously used in Ref. (7) to evaluate matrix elements of QED interaction vertices with newly-developed analytic methods.
3. To achieve improved convergence, we allow the HO basis length scale to be fixed separately in each Fock sector which allows a more efficient treatment of the transverse center-of-momentum degree of freedom.
4. We correct the evaluation of the anomalous magnetic moment  $a_e$  and a factor appearing in the vertex matrix elements. These corrections go in opposing directions for the previously evaluated  $a_e$  in an external trap (7) and updated results will be provided in a separate paper (40).

## 5. Results for electron anomalous magnetic moment $a_e$

With the methods and improvements summarized in Secs. 3 and 4, we evaluate and diagonalize the light-front QED Hamiltonian in  $|e\rangle$  and  $|e\gamma\rangle$  sectors without the external transverse trap and evaluate  $a_e$  from the resulting light-front amplitude for the lowest mass eigenstate.

In Ref. (7) the electron anomalous magnetic moment was approximated (based on non-relativistic quantum mechanics) by the squared modulus of the helicity-flip (for the constituent electron) components of the eigenstates. The precise definition of the electron anomalous magnetic moment in relativistic QED is  $a_e$ , the electron Pauli form factor  $F_2$  evaluated at momentum transfer  $q^2 \rightarrow 0$  (42),

$$a_e \equiv \frac{g-2}{2} = \lim_{q^2 \rightarrow 0} F_2(q^2). \quad (10)$$

In BLFQ the  $a_e$  can be calculated by sandwiching the operator corresponding to  $F_2(0)$  with the solution for the ground state for the electron with opposing helicities,

$$\begin{aligned}
 a_e &\equiv \frac{g-2}{2} = \langle \Psi_e^\downarrow | F_2(0) | \Psi_e^\uparrow \rangle \\
 &= \sum_{i',i} \langle \Psi_e^\downarrow | e\gamma, i' \rangle \langle e\gamma, i' | F_2(0) | e\gamma, i \rangle \langle e\gamma, i | \Psi_e^\uparrow \rangle.
 \end{aligned} \tag{11}$$

Here  $\langle e\gamma, i' | F_2(0) | e\gamma, i \rangle$  is the matrix element of the Pauli form factor in the BLFQ basis. The  $\langle e\gamma, i | \Psi_e^{\uparrow(\downarrow)} \rangle$  is the wavefunction of a physical electron with helicity up (down) in the  $|e\gamma\rangle$  sector (the only sector contributing to  $a_e$  in our truncated basis). The  $i$  denotes a complete set of quantum numbers. Although Eq.(11) involves two electron eigenstates with opposite helicities, in practice one needs only to solve for one of them and infer the other by exploiting the parity symmetry in light-front QED (43). The explicit expression for  $\langle e\gamma, i' | F_2(0) | e\gamma, i \rangle$  and the exact relation between  $\langle e\gamma, i | \Psi_e^\uparrow \rangle$  and  $\langle e\gamma, i | \Psi_e^\downarrow \rangle$  will be reported in a later work (40).

In this work without the external trap we reduce the QED coupling constant  $\alpha$  by a factor of  $10^4$  in order to reduce higher order effects and facilitate comparison with  $a_e$  from perturbation theory (44). In addition, we omit the instantaneous electron exchange vertex for the same reason.

We define our basis space with total longitudinal momentum  $K=80$  which we found adequate for the present application but will be extended in the future. In fact, the results presented in Ref. (10) already extend the basis to  $K=160$ . Furthermore, we use 2D HO single-particle states with frequencies  $\omega$  ranging from 0.01MeV to 1.4MeV. These  $\omega$ 's bracket the electron mass  $m_e=0.511$  MeV, the only scale-setting parameter in the QED Hamiltonian. At each  $\omega$  we calculate  $a_e$  with  $N_{\max}$  in the range of 10 to 118 to map out its convergence behavior with increasing  $N_{\max}$ . Larger  $N_{\max}$  translates to a larger basis with higher effective ultraviolet cutoff and lower effective infrared cutoff in the transverse plane. We expect that, with increasing  $N_{\max}$ , the results more closely approximate the Schwinger result. The rate of convergence may be different for different  $\omega$ 's, depending on  $a_e$ 's sensitivity to the effective cutoffs of the basis space. Our results agree with this expectation and approach the Schwinger result uniformly as  $N_{\max}$  increases with increments of 4.

In Fig. 8 I present the results evaluated with  $\omega=0.1$ MeV. For comparison, see the results in Ref. (10) at  $\omega=0.02$ MeV and  $\omega=0.5$ MeV. For each  $\omega$  the results exhibit a simple pattern with increasing  $N_{\max}$ : the results with even  $N_{\max}/2$  are systematically larger than those with odd  $N_{\max}/2$  so that the former and the latter separate into two individual groups. Within each group the results define a trend which is understandable by analysis of the perturbative calculation in light-front QED (10; 39; 40). Other features of these results are similarly understandable (10; 40).

The data points in Fig. 8 appear to define straight lines as a function of  $1/\sqrt{N_{\max}}$  as can be seen by the linear fits to all the points shown (solid lines). We can therefore easily extrapolate to the limit of no basis truncation ( $N_{\max} \rightarrow \infty$ ) where we expect to recover the Schwinger result. Indeed as seen in Fig. 8 the lines converge close to the Schwinger result in this limit. Their intercepts at  $1/N_{\max}=0$  are: 0.1131(1.0%) and 0.1133(1.4%) for even  $N_{\max}/2$  and odd  $N_{\max}/2$ , respectively. The percentages in the parenthesis are their corresponding relative deviation from the Schwinger result,  $\frac{a_e}{e^2} = \frac{\alpha}{2\pi e^2} = \frac{1}{8\pi^2} \approx 0.012665$ .

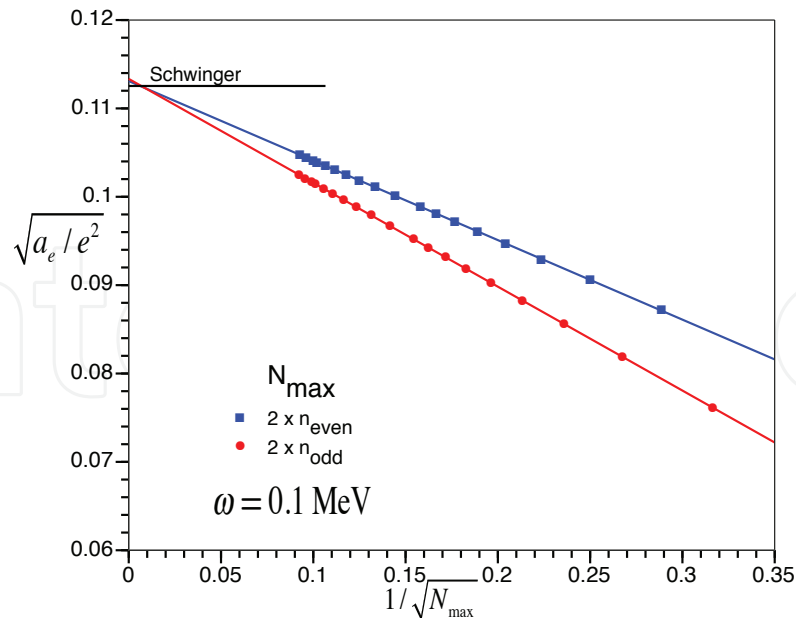


Fig. 8. (Color online) Anomalous magnetic moment of the electron calculated in BLFQ compared to the Schwinger result (44). The vertical axis is the square root of anomalous magnetic moment normalized to electron charge,  $e$ , so the Schwinger value is  $\sqrt{\frac{1}{8\pi^2}} = 0.11254$ . The horizontal axis is the square root of the reciprocal of  $N_{\max}$ . Symbols are for the BLFQ results. Squares: even  $N_{\max}/2$ ; circles: odd  $N_{\max}/2$ . The HO frequency for the basis is 0.1 MeV as indicated in the legend. The lines are linear extrapolations of BLFQ results based on all the points shown which span  $N_{\max} = 10 - 118$

What is not so apparent from a visual inspection of Fig. 8 is the fact that the extrapolated values come closer to the Schwinger result if one limits the linear fit to results for only the larger values of  $N_{\max}$ . For example, if the linear fit is performed for  $N_{\max} \geq 64$  the extrapolated values improve to 0.1129(0.7%) and 0.1130(0.9%) for even  $N_{\max}/2$  and odd  $N_{\max}/2$ , respectively. Continuing this avenue of investigation, if the linear fit is performed only for results with  $N_{\max} \geq 100$  the extrapolated values improve to 0.1128(0.4%) and 0.1129(0.6%) for even  $N_{\max}/2$  and odd  $N_{\max}/2$ , respectively. This is an encouraging sign of expected systematic improvement with increasing  $N_{\max}$ .

What is also important to note is that these results are systematically improvable. We will extend the calculations to larger  $K$  and  $N_{\max}$  values to further improve accuracy and reduce extrapolation uncertainties. That is, we will evaluate additional results in regions where they are expected to scale more accurately as a function of  $\sqrt{\frac{1}{N_{\max}}}$ . In order to compare with the perturbative result for  $a_e$  with the rescaling as shown in Fig. 8 (i.e. to achieve results for  $\frac{a_e}{e^2}$ ) it is also advantageous to further decrease the fine structure constant below  $10^{-4}\alpha$ , the value for the results presented here.

## 6. Conclusion

The recent history of light-front Hamiltonian field theory features many advances that pave the way for non-perturbative solutions of gauge theories. The goal is to evaluate the light-front

amplitudes for strongly interacting composite systems and predict experimental observables. High precision tests of the Standard Model may be envisioned as well as applications to theories beyond the Standard Model.

We can extend the BLFQ approach to QCD by implementing the SU(3) color degree of freedom for each parton - 3 colors for each fermion and 8 for each boson. We have investigated two methods for implementing the global color singlet constraint and we illustrate the resulting multiplicity of color configurations for each space-spin configuration in Fig. 9. In the first case, we follow Ref. (45) by constraining all color components to have zero color projection and adding a Lagrange multiplier term to the Hamiltonian to select global color singlet eigenstates. This produces the upper curves in each panel of Fig. 9. In the second case, we restrict the basis space to global color singlets (4–6; 46). The second method produces the lower curves in each panel of Fig. 9 and shows a factor of 30-40 lower many-parton basis space dimension at the cost of increased computation time for matrix elements. Either implementation provides an exact treatment of the global color symmetry constraint but the use of the second method provides overall more efficient use of computational resources. Nevertheless, the computational requirements of this approach are substantial, and we foresee extensive use of leadership-class computers to obtain practical results.

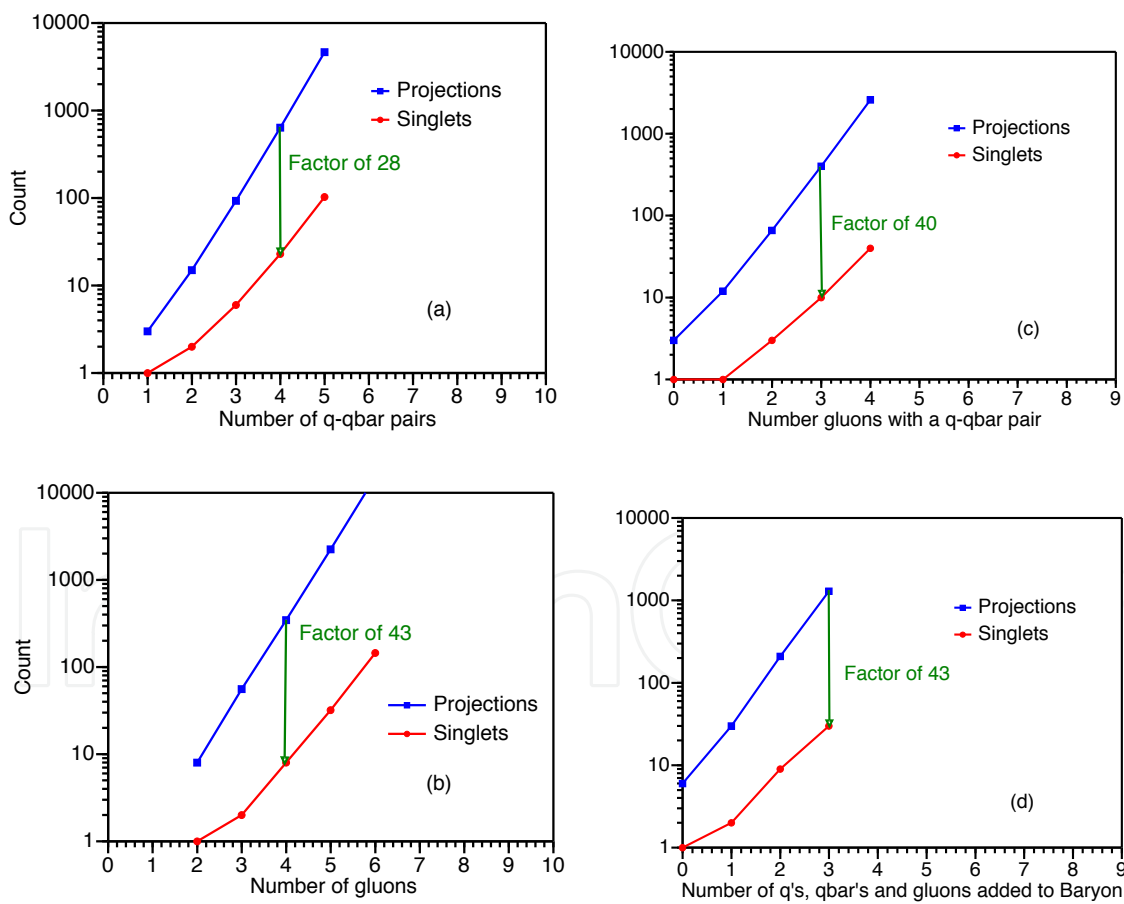


Fig. 9. (color online) Number of color space states that apply to each space-spin configuration of selected multi-parton states for two methods of enumerating the color basis states. The upper curves are counts of all color configurations with zero color projection. The lower curves are counts of global color singlets (adapted from Ref. (4)).

I would like to close by mentioning that we are extending the QED application in several directions. One specific goal is to include the capability for treating strong time-dependent laser pulses to address non-perturbative QED processes (35). In addition, we are launching an initial effort to evaluate the properties of charmonium in a BLFQ treatment of QCD with a first application to the heavy-quarkonia sector leading to predictions for the hybrid states (states dominated by  $q$ - $\bar{q}$ -glue configurations).

## 7. Acknowledgments

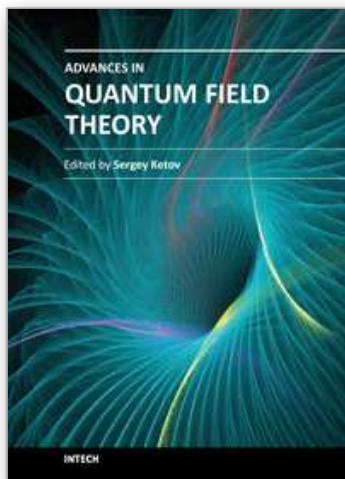
The author thanks all his collaborators on the cited publications as well as K. Tuchin, J. Hiller, S. Chabysheva, V. Karmanov, A. Ilderton, Y. Li and P. Wiecki for fruitful discussions. Computational resources were provided by the National Energy Research Scientific Computing Center (NERSC), which is supported by the Office of Science of the U.S. Department of Energy under Contract No. DE-AC02-05CH11231. This work was supported in part by US DOE Grants DE-FG02-87ER40371 and DE-FC02-09ER41582 (UNEDF SciDAC Collaboration). This work was also supported in part by US NSF grant 0904782.

## 8. References

- [1] H. C. Pauli and S. J. Brodsky, *Solving Field Theory In One Space One Time Dimension*, *Phys. Rev. D* 32, (1985)1993; S. J. Brodsky, H. C. Pauli and S. S. Pinsky, *Quantum Chromodynamics and Other Field Theories on the Light Cone*, *Phys. Reports* 301 (1998) 299 [*hep-ph/9705477*].
- [2] D. Chakrabarti, A. Harindranath and J. P. Vary, *A Study of  $q$ - $\bar{q}$  States in Transverse Lattice QCD Using Alternative Fermion Formulations*, *Phys. Rev. D* 69, (2004) 034502 [*hep-ph/0309317*].
- [3] D. Grunewald, E. M. Ilgenfritz, E. V. Prokhvatilov and H. J. Pirner, *Formulating Light Cone QCD on the Lattice*, *Phys. Rev. D* 77 (2008) 014512.
- [4] J. P. Vary, H. Honkanen, J. Li, P. Maris, S. J. Brodsky, A. Harindranath, G. F. de Teramond, P. Sternberg, E. G. Ng and C. Yang, *Hamiltonian light-front field theory in a basis function approach*, *Phys. Rev. C* 81,(2010) 035205.
- [5] J. P. Vary, H. Honkanen, Jun Li, P. Maris, S. J. Brodsky, A. Harindranath, G. F. de Teramond, P. Sternberg, E. G. Ng, C. Yang, *Hamiltonian light-front field theory within an AdS/QCD basis*, *Nucl. Phys. B* 199, 64 (2010).
- [6] J. P. Vary, H. Honkanen, Jun Li, P. Maris, A. M. Shirokov, S. J. Brodsky, A. Harindranath, G. F. de Teramond, P. Sternberg, E. G. Ng, C. Yang and M. Sosonkina, *Ab initio Hamiltonian approach to light nuclei and to quantum field theory*, *Pramana Jnl of Phys.* 75, 39 (2010).
- [7] H. Honkanen, P. Maris, J. P. Vary and S. J. Brodsky, *Electron in a transverse harmonic cavity*, *Phys. Rev. Lett.* 106, 061603 (2011).
- [8] J. P. Vary, *Non-Perturbative Hamiltonian Light-Front Field Theory: Progress and Prospects*, *Proceedings of Science*, PoS(LC2010)001 (available online).
- [9] J. P. Vary, *Hamiltonian Light-Front Field Theory: Recent Progress and Tantalizing Prospects*, *Few-Body Systems* (to appear), 2012; arXiv:1110.1071.
- [10] X. Zhao, H. Honkanen, P. Maris, J. P. Vary and S. J. Brodsky *Electron Anomalous Magnetic Moment in Basis Light-Front Quantization Approach*, *Few-Body Systems* (to appear), 2012; arXiv:1110.0553.
- [11] P. Navrátil, J. P. Vary and B. R. Barrett, *Properties of  $^{12}\text{C}$  in the ab-initio Nuclear Shell Model*, *Phys. Rev. Lett.* 84 (2000) 5728; *Large-basis ab-initio No-core Shell Model and its application to  $^{12}\text{C}$* , *Phys. Rev. C* 62 (2000) 054311.

- [12] P. Maris, J. P. Vary and A. M. Shirokov, *Ab Initio no-core full configuration calculations of light nuclei*, *Phys. Rev. C* 79 (2009) 014308 [nucl-th/0808.3420].
- [13] A. C. Hayes, P. Navrátil and J. P. Vary, *Neutrino-12C Scattering in the ab initio Shell Model with a Realistic Three-Body Interaction* *Phys. Rev. Lett.* 91, 012502 (2003); nucl-th/0305072.
- [14] A. M. Shirokov, J. P. Vary, A. I. Mazur and T. A. Weber, *Realistic Nuclear Hamiltonian: Ab exitu approach*, *Phys. Letts. B* 644 (2007) 33 [nucl-th/0512105].
- [15] P. Navratil, V. G. Gueorguiev, J. P. Vary, W. E. Ormand and A. Nogga, *Structure of  $A = 10-13$  nuclei with two- plus three-nucleon interactions from chiral effective field theory*, *Phys. Rev. Lett.* 99 (2007)042501 [nucl-th/0701038].
- [16] P. Maris, M. Sosonkina, J. P. Vary, E. G. Ng and C. Yang, *Scaling of ab-initio nuclear physics calculations on multicore computer architectures*, International Conference on Computer Science, ICCS 2010, *Procedia Computer Science* 1 (2010) 97.
- [17] P. Maris, J. P. Vary, P. Navratil, W. E. Ormand, H. Nam, D. J. Dean, *Origin of the anomalous long lifetime of  $^{14}\text{C}$* , *Phys. Rev. Lett.* 106, 202502(2011).
- [18] B. R. Barrett, P. Navratil and J. P. Vary, *Ab initio No Core Shell Model*, *Nuclear Physics News International*, 21, 5 (2011).
- [19] S. K. Bogner, R. J. Furnstahl, P. Maris, R. J. Perry, A. Schwenk and J. P. Vary, *Convergence in the no-core shell model with low-momentum two-nucleon interactions*, *Nucl. Phys. A* 801, (2008) 21[nucl-th/0708.3754].
- [20] P. Maris, A. M. Shirokov and J. P. Vary, *Ab initio nuclear structure simulations: the speculative  $^{14}\text{F}$  nucleus*, *Phys. Rev. C* 81 (2010) 021301(R).
- [21] A. Negret, et al., *Gamow-Teller Strengths in the  $A = 14$  Multiplet: A Challenge to the Shell Model*, *Phys. Rev. Lett.* 97, 062502 (2006).
- [22] S. Quaglioni and P. Navrátil, *Phys. Rev. Lett.* 101, 092501 (2008).
- [23] S. Quaglioni and P. Navrátil, *Phys. Rev. C* 79, 044606 (2009).
- [24] K. Wildermuth and Y. C. Tang, *A unified theory of the nucleus* (Vieweg, 1977, Braunschweig).
- [25] D. Chakrabarti, A. Harindranath, L. Martinovic and J. P. Vary, *Kinks in discrete light cone quantization*, *Phys. Lett. B* 582, (2004) 196 [arXiv:hep-th/0309263].
- [26] D. Chakrabarti, A. Harindranath, L. Martinovic, G. B. Pivovarov and J. P. Vary, *Ab initio results for the broken phase of scalar light front field theory*, *Phys. Lett. B* 617, (2005) 92 [arXiv:hep-th/0310290].
- [27] D. Chakrabarti, A. Harindranath and J. P. Vary, *A transition in the spectrum of the topological sector of  $\phi^{*4}(2)$  theory at strong coupling*, *Phys. Rev. D* 71, (2005) 125012 [arXiv:hep-th/0504094].
- [28] S. J. Brodsky, V. A. Franke, J. R. Hiller, G. McCartor, S. A. Paston and E. V. Prokhvatilov, *A nonperturbative calculation of the electron's magnetic moment*, *Nucl. Phys. B* 703 (2004) 333;
- [29] S. S. Chabysheva and J. R. Hiller, *A nonperturbative calculation of the electron's magnetic moment with truncation extended to two photons*, *Phys. Rev. D* 81 (2010) 074030;
- [30] S. S. Chabysheva and J. R. Hiller, *On the nonperturbative solution of Pauli–Villars-regulated light-front QED: A comparison of the sector-dependent and standard parameterizations*, *Annals Phys.* 325 (2010) 2435.
- [31] S. Dalley and B. van de Sande, *Transverse lattice calculation of the pion light-cone wavefunctions*, *Phys. Rev. D* 67 (2003) 114507, [arXiv:hep-ph/0212086].
- [32] S. J. Brodsky, D. Chakrabarti, A. Harindranath, A. Mukherjee and J. P. Vary, *Hadron optics: Diffraction patterns in deeply virtual Compton scattering*, *Phys. Lett. B* 641, (2006) 440 [arXiv:hep-ph/0604262]; S. J. Brodsky, D. Chakrabarti, A. Harindranath, A. Mukherjee

- and J. P. Vary, *Hadron optics in three-dimensional invariant coordinate space from deeply virtual Compton scattering*, *Phys. Rev. D* 75, 014003 (2007) [arXiv:hep-ph/0611159].
- [33] M. Ruf, G. R. Mocken, C. Muller, K. Z. Hatsagortsyan and C. H. Keitel, *Pair production in laser fields oscillating in space and time*, *Phys. Rev. Lett.* 102 (2009) 080402.
- [34] C. K. Dumlu and G. V. Dunne, *The Stokes Phenomenon and Schwinger Vacuum Pair Production in Time-Dependent Laser Pulses*, *Phys. Rev. Lett.* 104 (2010) 250402,
- [35] A. Ilderton, *Trident pair production in strong laser pulses*, *Phys. Rev. Lett.* 106, 020404 (2011).
- [36] A. Adare *et al.* [PHENIX Collaboration], *Detailed Measurement Of The  $E^+E^-$  Pair Continuum In  $P + P$  And  $Au+Au$  Collisions At  $\sqrt{s_{NN}} = 200$  Gev And Implications For Direct Photon Production*, *Phys. Rev. C* 81 (2010) 034911.
- [37] K. Tuchin, *Photon decay in strong magnetic field in heavy-ion collisions*, *Phys. Rev. C* 83, 017901 (2011).
- [38] G. F. de Teramond and S. J. Brodsky, *Light-Front Holography: A First Approximation to QCD*, *Phys. Rev. Lett.* 102, 081601 (2009).
- [39] S. J. Brodsky and G. F. de Teramond, *Light-Front hadron dynamics and AdS/CFT correspondence*, *Phys. Lett. B* 582 (2004) 211 [hep-th/0310227]; A. Karch, E. Katz, D. T. Son and M. A. Stephanov, *Linear confinement and AdS/QCD*, *Phys. Rev. D* 74, (2006)015005.
- [40] X. Zhao, H. Honkanen, P. Maris, J. P. Vary and S. J. Brodsky, *Electron in a transverse harmonic cavity*, in preparation.
- [41] V. A. Karmanov, J.-F. Mathiot and A. V. Smirnov, *Systematic renormalization scheme in light-front dynamics with Fock space truncation*, *Phys. Rev. D* 77 (2008) 085028 [hep-th/0801.4507]
- [42] S. J. Brodsky and S. D. Drell, *The Anomalous Magnetic Moment and Limits on Fermion Substructure*, *Phys. Rev. D* 22, 2236 (1980).
- [43] S. J. Brodsky, S. Gardner and D. S. Hwang, *Discrete symmetries on the light front and a general relation connecting nucleon electric dipole and anomalous magnetic moments*, *Phys. Rev. D* 73, 036007 (2006).
- [44] J. S. Schwinger, *On Quantum Electrodynamics And The Magnetic Moment Of The Electron*, *Phys. Rev.* 73 (1948) 416.
- [45] R. J. Lloyd and J. P. Vary, *All-charm Tetraquarks*, *Phys. Rev. D* 70 (2004) 014009 [hep-ph/0311179].
- [46] Jun Li, *Light front Hamiltonian and its application in QCD* Ph. D. thesis, Iowa State University (2009), unpublished.



## **Advances in Quantum Field Theory**

Edited by Prof. Sergey Ketov

ISBN 978-953-51-0035-5

Hard cover, 230 pages

**Publisher** InTech

**Published online** 03, February, 2012

**Published in print edition** February, 2012

Quantum Field Theory is now well recognized as a powerful tool not only in Particle Physics but also in Nuclear Physics, Condensed Matter Physics, Solid State Physics and even in Mathematics. In this book some current applications of Quantum Field Theory to those areas of modern physics and mathematics are collected, in order to offer a deeper understanding of known facts and unsolved problems.

### **How to reference**

In order to correctly reference this scholarly work, feel free to copy and paste the following:

James P. Vary (2012). Ab Initio Hamiltonian Approach to Light-Front Quantum Field Theory, *Advances in Quantum Field Theory*, Prof. Sergey Ketov (Ed.), ISBN: 978-953-51-0035-5, InTech, Available from: <http://www.intechopen.com/books/advances-in-quantum-field-theory/ab-initio-hamiltonian-approach-to-light-front-quantum-field-theory>

**INTECH**  
open science | open minds

### **InTech Europe**

University Campus STeP Ri  
Slavka Krautzeka 83/A  
51000 Rijeka, Croatia  
Phone: +385 (51) 770 447  
Fax: +385 (51) 686 166  
[www.intechopen.com](http://www.intechopen.com)

### **InTech China**

Unit 405, Office Block, Hotel Equatorial Shanghai  
No.65, Yan An Road (West), Shanghai, 200040, China  
中国上海市延安西路65号上海国际贵都大饭店办公楼405单元  
Phone: +86-21-62489820  
Fax: +86-21-62489821

© 2012 The Author(s). Licensee IntechOpen. This is an open access article distributed under the terms of the [Creative Commons Attribution 3.0 License](#), which permits unrestricted use, distribution, and reproduction in any medium, provided the original work is properly cited.

IntechOpen

IntechOpen